JACS
JOURNAL OF THE AMERICAN CHEMICAL SOCIETY
pubs.acs.org/JACS
Article

Construction of Nanomotors with Replaceable Engines by Supramolecular Machine-Based Host–Guest Assembly and Disassembly

Zihan Ye, Yong Wang, Sanhu Liu, Dandan Xu, Wei Wang, and Xing Ma*

Cite This: J. Am. Chem. Soc. 2021, 143, 15063–15072
Read Online

ACCESS | Metrics & More | Article Recommendations | Supporting Information

ABSTRACT: Micro/nanomotors (MNMs) are miniaturized devices capable of performing self-propelled motion and on-demand tasks, which have brought revolutionary renovations in nanomedicine, environmental remediation, biochemical sensing, etc. Numerous methods of either chemical synthesis or physical fabrications have been extensively investigated to prepare MNMs of various shapes and functions. However, MNMs with replaceable engines that can be flexibly assembled and disassembled, resembling that of a macroscopic machine, have not been achieved. Here, for the first time, we report a demonstration of control over the engine replacement of self-propelled nanomotors based on hollow mesoporous silica nanoparticles (HMSNPs) via supramolecular machine-based host–guest assembly and disassembly between azobenzene (Azo) and β-cyclodextrin (β-CD). Nanomotors with different driving mechanisms can be rapidly constructed by selecting corresponding β-CD-modified nanoengines of urease, Pt, or Fe_3O_4, to assemble with the azobenzene-modified HMSNPs (HMSNPs-Azo). In virtue of photoresponsive *cis*/*trans* isomer conversion of azobenzene molecules, engine switching can be accomplished by remote light triggered host–guest assembly or disassembly between HMSNPs-Azo and β-CD-modified engines. Moreover, this method can quickly include multiple engines on the surface of the HMSNPs-Azo to prepare a hybrid MNM with enhanced motion capability. This strategy not only is cost-effective for the rapid and convenient preparation of nanomotors with different propulsion mechanism but also paves a new path to future multiple functionalization of MNMs for on-demand task assignment.

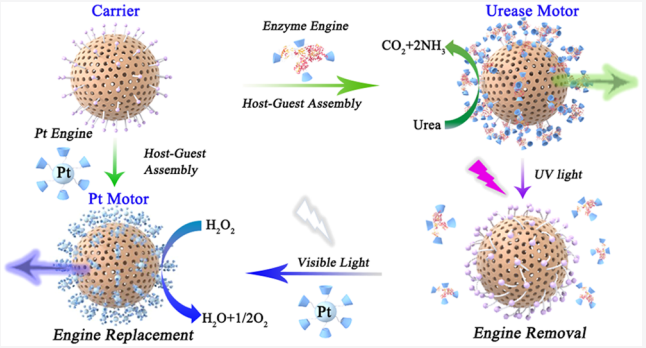

INTRODUCTION

Nature has created biological motors capable of performing complex tasks with precision by converting chemical energy into mechanical work,[1,2] which has inspired developments of artificial micro/nanomotors (MNMs) to mimic their autonomous motion and functions at a small scale. These synthetic MNMs are micro- or nanoscale mobile devices that can covert energies from chemical fuels or external physical fields into mechanical force to achieve active movement and accomplish on-demand tasks.[3−5] Over the past decade, MNMs have experienced significant advances with potential revolutionary applications demonstrated in many fields, such as drug delivery,[6−8] cargo transportation,[9,10] biochemical sensing,[11,12] micro/nanosurgery,[13,14] and environmental remediation.[15,16]

Up to now, plenty of strategies and techniques have been explored for the design and fabrication of MNMs,[17,18] such as chemical synthesis,[19−21] electrochemical deposition,[22,23] physical vapor deposition,[24,25] photolithography,[26] microfluidic technology,[27] layer-by-layer assembly,[28,29] and 3-D printing, such as direct laser writing.[30] Usually, the activation of the self-propelled MNMs requires the introduction of chemically or physically active components, named as "engines" here, such as catalytic materials (e.g., Pt, MnO_2) for many chemically powered MNMs,[23,31] and magnetic materials (e.g., Fe_3O_4 nanoparticles, Ni, Co) for magnetic MNMs.[32] These engines are responsible for energy conversion for self-propulsion of MNMs. However, most of these driving engines are usually permanently "fixed" onto the surface of the carrier structure of MNMs, *e.g.*, by a chemical bond or physical deposition, which cannot be replaced once they are immobilized onto MNMs. Such a situation results in several apparent disadvantages. First of all, the propulsion mechanism of as-prepared MNMs is predefined, which limits their adaptability toward the change of surrounding circumstances such as fuel depletion. Furthermore, any damage to the driving engine (such as

Received: May 10, 2021
Published: September 9, 2021

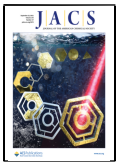

Downloaded via UNIV TOWN OF SHENZHEN on November 1, 2021 at 02:56:26 (UTC).
See https://pubs.acs.org/sharingguidelines for options on how to legitimately share published articles.

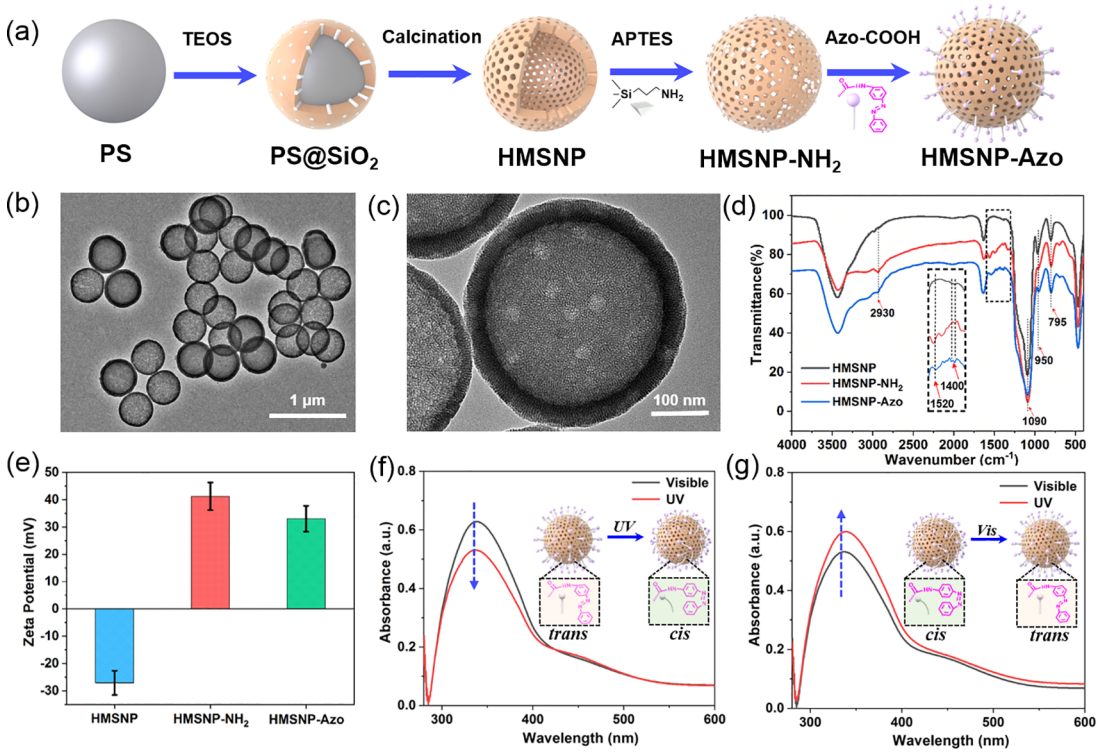

Figure 1. Fabrication and characterization of the main carrier (HMSNP-Azo) of the nanomotors. (a) Schematic illustration of the synthesis route of HMSNP-Azo. (b, c) TEM images of HMSNP. (d) FT-IR spectra of HMSNP, HMSNP-NH_2, and HMSNP-Azo. (e) Zeta potential of HMSNP (blue), HMSNP-NH_2 (red), and HMSNP-Azo (green). UV−vis adsorption spectra of HMSNP-Azo upon light irradiation of different wavelengths: (f) from visible to UV light and (g) from UV to visible light. Error bars indicate standard deviation (N = 5).

denaturization of enzymes and catalyst poisoning) would lead to the permanent failure of the MNMs, which cannot be reused anymore. Last, different fabrication strategies need to be developed for the introduction of a specific engine, which requires many more processing steps for multifunctionalization of MNMs. However, it is common sense that machines of the macroscopic world are composed of functional units or parts integrated through mechanical assembly. We only need to replace the damaged part, like an engine for a car, to "fix" a failed machine. So, we wondered whether we can construct self-propelled nanomotors with replaceable engines that can be mechanically assembled and disassembled, resembling macroscopic machines from a molecular level. Such a strategy would greatly expand the flexibility and adaptability of MNMs.

The 2016 Nobel Prize in Chemistry awarded the invention of a "molecular machine",[33] which refers to mechanical assembly of at least two different molecular units at the sub-nanoscale, such as mechanically interlocked systems of rotaxanes or catenanes.[34,35] As a fundamental building block, "molecular machines" have experienced tremendous progress regarding the development of smart materials, as well as useful applications in many fields, such as controlled drug delivery,[36] bioimaging,[37] and catalysis.[38] Host−guest interactions have played a pivotal role for molecular machines,[39] which form a mechanical interlock between host molecules such as cyclodextrin (CD), cucurbituril (CB), and calixarene (CA), with a variety of guest moieties by supramolecular hydrophobic/hydrophilic interactions.

These supramolecular machine-based mechanical assemblies are stimuli-responsive, which allows for control over their assembly and disassembly by applying external stimuli such as redox potential, pH, and even light.[40,41] Therefore, we expect that the toolbox of "supramolecular machines" of host−guest interactions will shed light on the construction of a nanomotor with replaceable engines that can be "installed" or "dismounted" on-demand at the molecular scale.

Hereby, we present the facile construction of nanomotors with replaceable engines by means of supramolecular machine-based host−guest assembly and disassembly. The main carrier of the assembled nanomotors is made of azobenzene-modified hollow mesoporous silica nanoparticle (HMSNP-Azo). Through host−guest interaction between azobenzene molecules on the HMSNPs and three β-CD-modified driving engines, corresponding nanomotors of varied propulsion mechanisms can be quickly produced and realize flexible replacement of different propelling engines. The current strategy provides a facile method to construct self-propelling nanomotors equipped with on-demand engines, which can readily adapt to different swimming environments or application scenarios.

RESULTS AND DISCUSSION

Synthesis and Characterization of the Carrier Part of Nanomotors (HMSNP-Azo). As shown in Figure 1(a), we first prepared HMSNP using monodispersed polystyrene nanoparticles (PS) as a sacrificial template according to the previous report.[42] Next, the HMSNP was modified with 3-aminopropyl triethoxysilane (APTES), denoted as HMSNP-NH_2. The synthetic carboxylated azobenzene molecules (Azo-COOH) (see Experimental Section in the SI) were further covalently bonded to the surface of HMSNP through an imitation reaction with amino groups ($-NH_2$) to produce HMSNP-Azo, which was used as the carrier part of the following nanomotors. The HMSNPs were characterized by

https://doi.org/10.1021/jacs.1c04836
J. Am. Chem. Soc. 2021, 143, 15063−15072

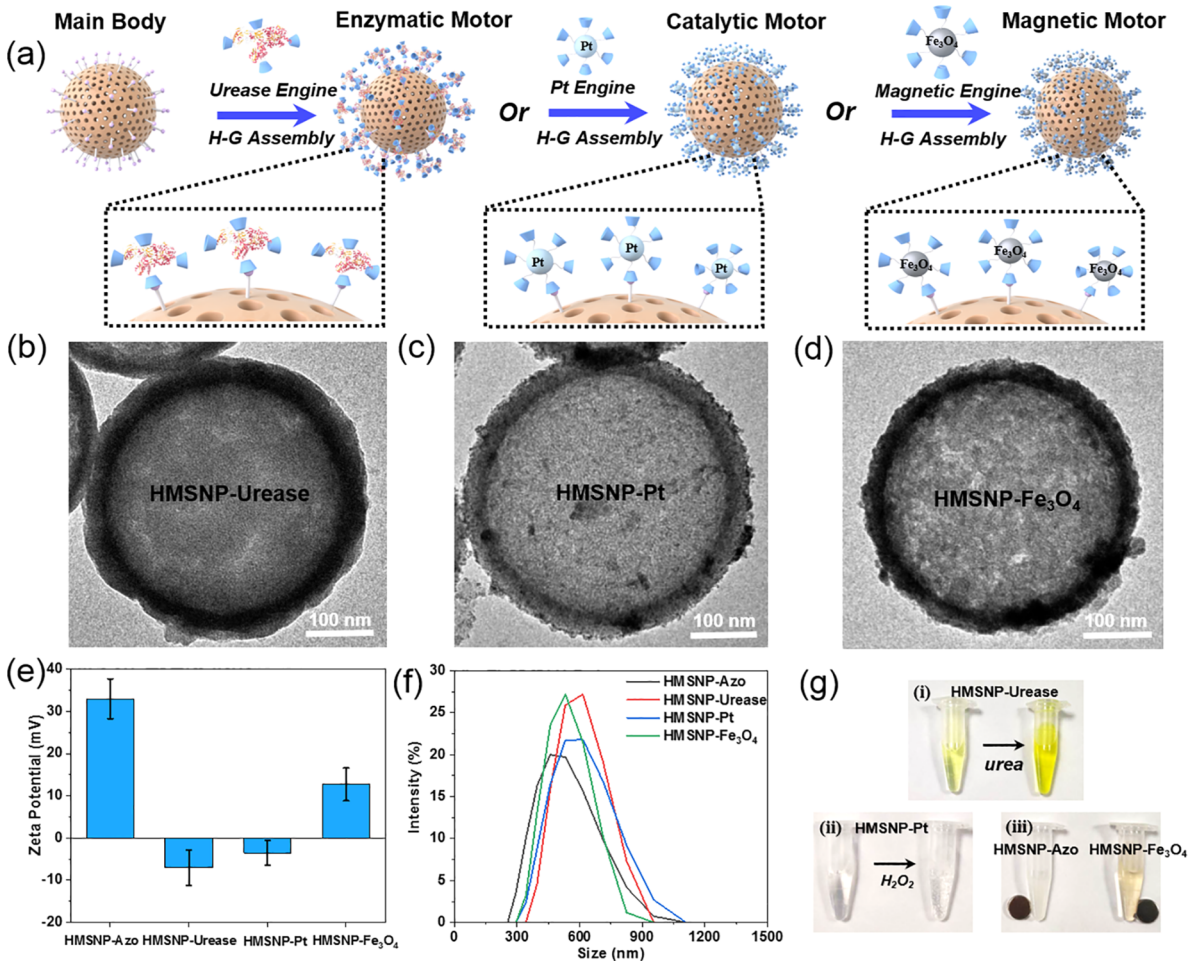

Figure 2. Host−guest interaction induced mechanical assembly of the corresponding nanomotors. (a) Schematic illustration of the self-assembly process enabled construction of corresponding nanomotors. (b−d) TEM images of typical HMSNP-Urease, HMSNP-Pt, and HMSNP-Fe_3O_4 nanomotors. (e) Zeta potential and (f) hydrodynamic size distribution of the HMSNP-Azo, HMSNP-Urease, HMSNP-Pt, and HMSNP-Fe_3O_4 nanoparticles. Error bars indicate standard deviation (N = 5). (g) Catalytic activity test of HMSNP-Urease (i) and HMSNP-Pt (ii) and magnetic separation test of HMSNP-Fe_3O_4 (iii).

transmission electron microscopy (TEM) (Figure 1(b) and (c)), dynamic light scattering (DLS), and scanning electron microscopy (SEM) (Figure S1b). These results show that the HMNSPs have a uniform diameter of 402 ± 13 nm (average size ± standard deviation (SD), N = 50) and a hollow cavity with mesoporous shell structure. Meanwhile, we also demonstrated the surface modification process of the HMSNPs by Fourier-transformed infrared (FT-IR) spectrum and zeta potential measurement. As illustrated in Figure 1(d), the characteristic peaks of the HMSNPs at 795 and 1090 cm^{-1} are attributed to the symmetric and asymmetric stretching vibration of Si−O, respectively, and the peak at 950 cm^{-1} is due to the asymmetric vibration of Si−OH. After the surface modification by APTES, the peak at 1520 cm^{-1} from the amino group was found in HMSNP-NH_2. Upon further introduction of azobenzene molecules, a new peak appears at 1400 cm^{-1} from the amide carbonyl in HMSNP-Azo, indicating that the azobenzene molecules are successfully fixed on the surface of HMSNP. The reverse of the zeta potentials from −27 mV for HMSNP to 41 mV for HMSNP-NH_2 demonstrates the successful amination (Figure 1(e)). However, the surface charge of HMSNP-Azo is significantly lower than that of HMSNP-NH_2 due to further introduction of azobenzene groups. These results confirm the successful functionalization of HMSNP as demanded.

Subsequently, we investigated the reversible light-responsiveness behavior of HMSNP-Azo through UV−vis absorption spectrum measurement. As shown in Figure 1(f) and (g), an obvious characteristic peak was observed at 320 nm in the adsorption spectra of the HMSNP-Azo. When irradiated with ultraviolet (UV) light, the absorption peak at 320 nm showed a significant decrease (Figure 1(f)). This phenomenon was mainly due to the weakened absorption of the electron transition ($\pi-\pi^*$) in the *trans* isomer in the ultraviolet region, indicating that *trans* isomers were converted to *cis* isomers.[43] In contrast, the *cis* isomers generated in this way can be switched to *trans* isomers again upon visible light irradiation, which led to the intensity of the adsorption peak increasing (Figure 1(g)). These results are consistent with previous literature reports.[44] Therefore, we confirm that azobenzene molecules modifying the surface of the HMSNPs exhibit good reversible light-responsiveness. The successful fabrication of the carrier part of nanomotors, namely, HMNSP-Azo, allows for the further preparation of various nanomotors by host−guest supramolecular self-assembly.

Versatile Construction of Nanomotors by Supramolecular Host−Guest Assembly. In order to prepare

https://doi.org/10.1021/jacs.1c04836
J. Am. Chem. Soc. 2021, 143, 15063−15072

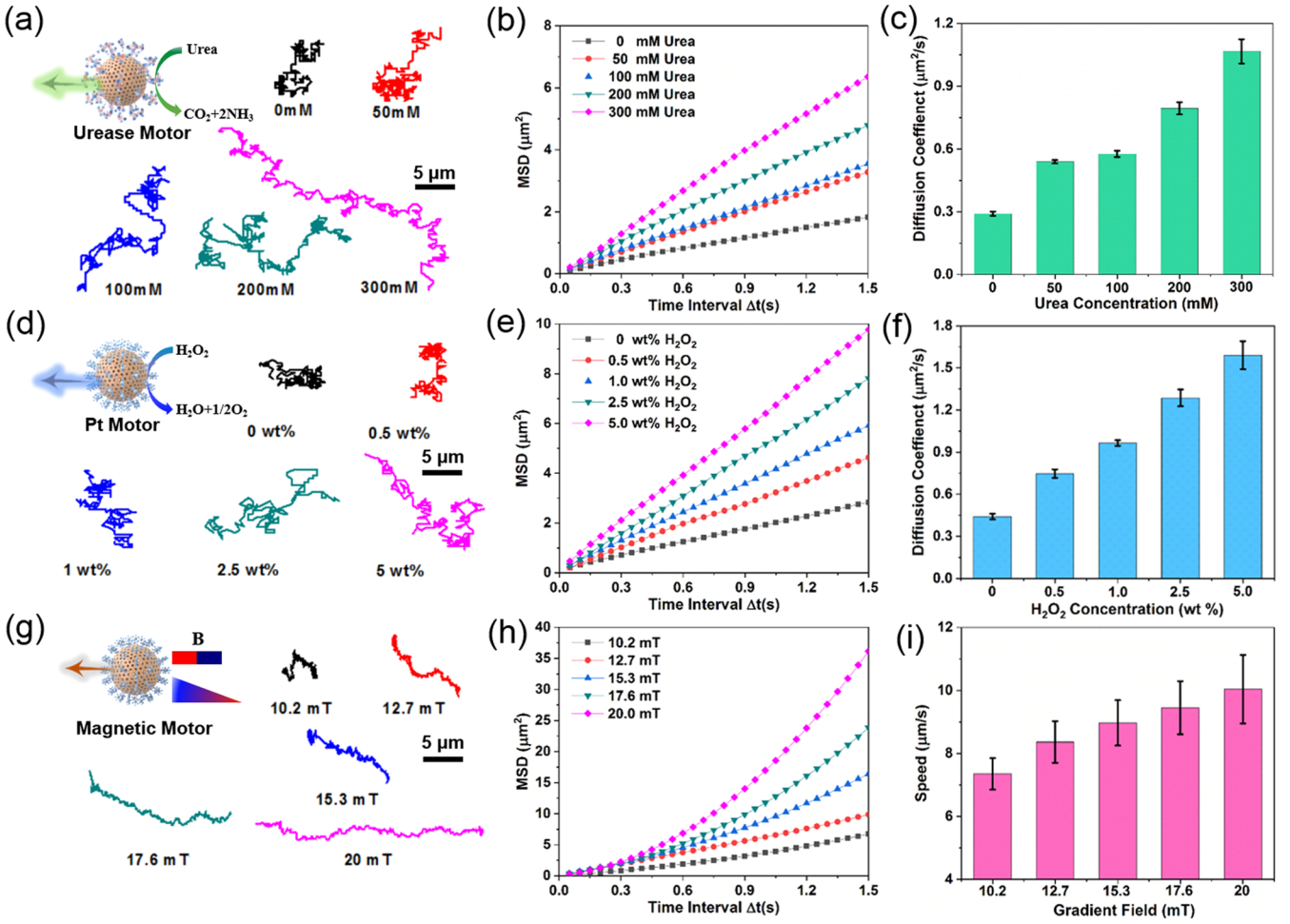

Figure 3. Active movement behavior of the corresponding nanomotors. (a, d, g) Representative tracking trajectories during 15 s; (b, e, h) average MSD of the urease motors, Pt motors, and magnetic motors. (c, f) Diffusion coefficient values determined from average MSD plots of the urease motors and Pt motors in (b) and (e), respectively. (i) Speed of the magnetic motors driven by a gradient magnetic field (measured at the motors' site). Error bars indicate standard deviation (N = 15).

nanomotors with different propelling nanoengines by using the obtained HMSNPs-Azo as the carrier, we first synthesized three kinds of β-CD-modified nanoengines here (see Experimental Section in the SI), namely, a urease engine (β-CD@Urease), a Pt engine (β-CD@Pt), and a magnetic engine (β-CD@Fe_3O_4). The synthesis and characterizations of these three nanoengines are described in detail in Figures S3−S6 in the SI. Then, three kinds of nanoengines were added into aqueous dispersions of HMSNPs-Azo, respectively. The supramolecular machine-based host−guest (H-G) interaction between azobenzene on the carriers and β-CD on the nanoengines would form inclusion complexes, which could mechanically assemble as-prepared nanoengines on the external surface of the carriers to yield corresponding nanomotors. The produced enzymatic motor of HMSNP-Urease, catalytic motor of HMSNP-Pt, and magnetic motor of HMSNP-Fe_3O_4 equipped with different driving nanoengines are schematically illustrated in Figure 2(a).

To further prove the successful preparation of these three kinds of nanomotors, we first characterized HMSNP-Urease, HMSNP-Pt, and HMSNP-Fe_3O_4 nanomotors by TEM. As shown in Figure 2(b), the surface of HMSNPs after urease modification is obviously blurred, and the mesopore channels can no longer be clearly distinguished as compared to the unmodified HMSNPs, preliminarily indicating that urease molecules were loaded onto the external surface. As seen in Figure 2(c) and (d), the surface of HMSNP-Pt and HMSNP-Fe_3O_4 becomes very rough and many relatively small nanoparticles appear due to the presence of self-assembled nanoengines. At the same time, we also found a uniform distribution of representative element of S (characteristic element for urease), Pt, and Fe on the surface of corresponding nanomotors by an energy dispersive spectrometer (EDX) (see Figure S(8)−S(10) in the SI). These results indicate that the urease engine, Pt engine, and magnetic engine were all linked onto the surface of HMSNP through host−guest inclusion complexes between β-CD and azobenzene molecules. In addition, zeta potential and DLS measurements were used to verify the preparation process of these aforesaid nanomotors as shown in Figure 2(e) and (f). Compared with the surface potential of HMSNP-Azo (33 mV), the potential of HMSNP-Urease, HMSNP-Pt, and HMSNP-Fe_3O_4 changed to −8, −3.5, and 12 mV, respectively, which is mainly due to the introduction of the urease engine, Pt engine, and magnetic engine with varied potentials (−11, −37, and 10 mV, respectively) (see Figure S6 in the SI). Here, the change of the zeta potential shows that three kinds of nanoengines are assembled on the surface of the carriers, separately. In addition, the hydrodynamic size of HMSNP-Urease, HMSNP-Pt, and HMSNP-Fe_3O_4 measured by DLS shows an apparent increase

https://doi.org/10.1021/jacs.1c04836
J. Am. Chem. Soc. 2021, 143, 15063−15072

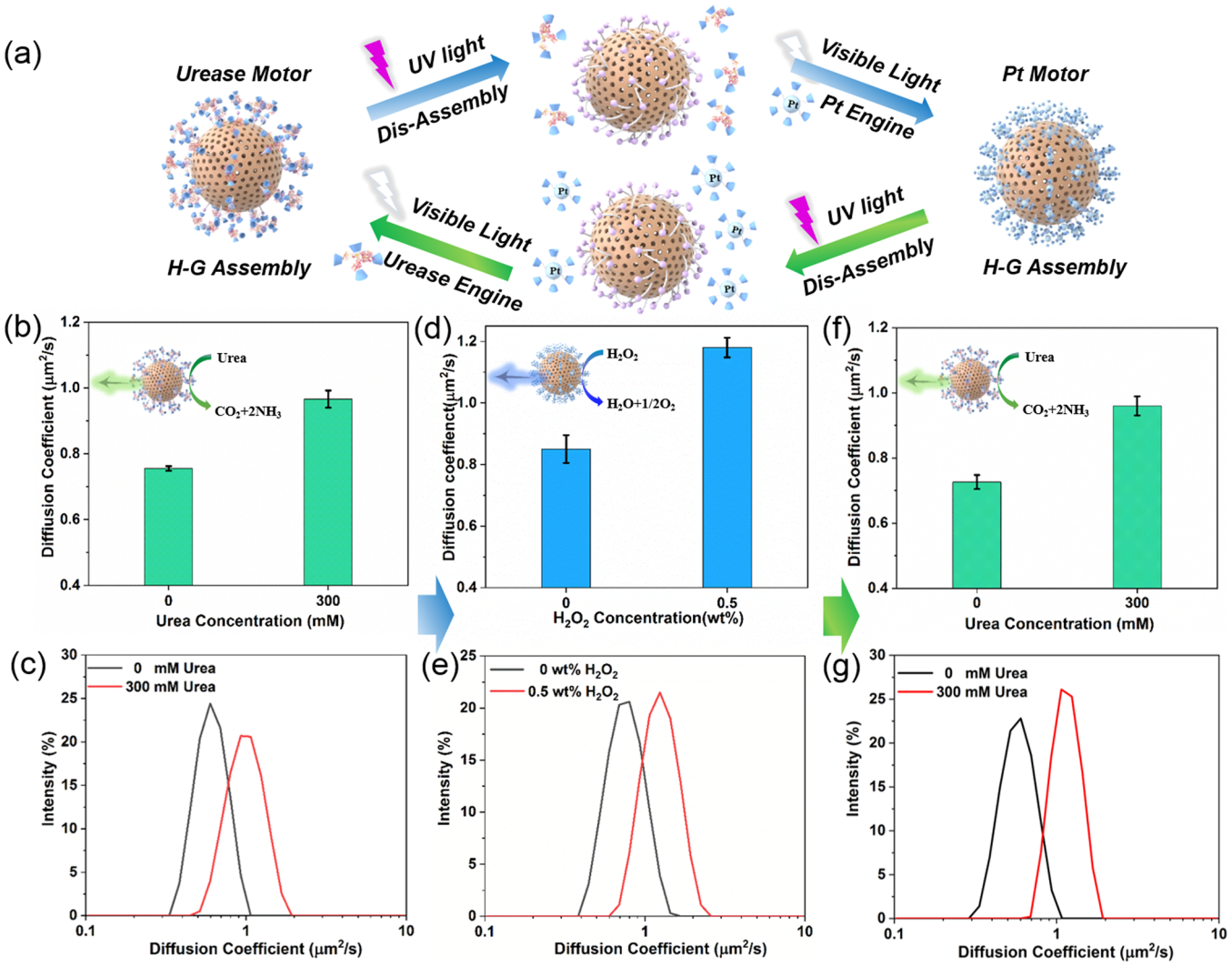

Figure 4. Cyclic switching of the nanoengine by light-responsive disassembly and reassembly of host−guest interactions. (a) Schematic illustration of disassembly and reversible assembly of nanoengines to achieve switching between a urease motor and a Pt motor through UV and visible light irradiation in turn. Diffusion coefficient and distribution (by DLS) of (b, c) the initial urease motor, (d, e) the Pt motor after switching Pt engines, (f, g) the urease motor after reassembling the urease engine again. Error bars indicate standard deviation (N = 10).

as compared with that of HMSNP-Azo before assembly. Finally, we conducted a preliminary test on the functions of each nanoengine after being assembled onto the nanomotors. As shown in Figure 2(g), in order to test the enzymatic activity of HMSNP-Urease, we first prepared a reaction solution containing HMSNP-Urease and *p*-nitrophenol and then added the urea or DI H_2O as control to the previous solution quickly. The solution of the enzyme-coupled hollow nanoparticles became bright yellow due to the formation of NH_4^+ that reacted with *p*-nitrophenol to yield a color change (Figure 2(g, i)), indicating that HMSNP-Urease exhibits obvious catalytic activity. We further evaluated the enzymatic activity of ureases immobilized on the HMSNPs by using a commercial urease activity assay kit. The activity of immobilized urease is found to be 1.15 U/mg and represents an enzymatic activity of 77.33% compared to that of the free enzyme (1.5 U/mg), which is in good agreement with the previous report.[45] Similarly, H_2O_2 was added to the prepared HMSNP-Pt suspension quickly, and a large number of bubbles were formed in the solution as HMSNP-Pt catalyzed the decomposition of H_2O_2 to produce oxygen gas (Figure 2(g, ii)), which shows that assembled platinum nanoengines still have good catalytic performance. The magnetic separation test indicates that the HMSNP-Fe_3O_4 nanomotors possess good magnetic responsiveness (Figure 2(g, iii)). Up to now, all results together demonstrate the successful construction of HMSNP-based urease motors, Pt motors, and magnetic motors by the supramolecular-based mechanical assembly of various nanoengines.

Motion Behavior of Self-Assembled Nanomotors Driven by Different Nanoengines. We first carried out motion analysis on the active movement behavior of the first two biocatalytic/catalytic nanomotors of HMSNP-Urease and HMSNP-Pt by optical microscopy and DLS, as shown in Figure 3. As previously reported,[46] in the presence of urea fuel, urease molecules binding to the surface of MNMs can catalyze the decomposition of urea into carbon dioxide and ammonia to achieve self-propulsion of MNMs by an ionic diffusion phoresis mechanism. The results of the corresponding motion trajectory of the Urease motors with different urea concentrations are shown in Figure 3(a). The movement of urease motors at 0 mM urea exhibited the typical Brownian motion, while with the presence of urea the area covered by

https://doi.org/10.1021/jacs.1c04836
J. Am. Chem. Soc. 2021, 143, 15063−15072

the trajectories is much larger than that without urea, suggesting enhanced diffusion of the urease motors, which is in agreement with previously reported urease-powered motors.[45] Based on the trajectories, MSD plots of the urease motors with different concentrations of urea were extracted and showed a linear relationship with the time interval (Δt) in Figure 3(b). In addition, the effective diffusion coefficient (D_e) was obtained by fitting the resulting MSD according to the equation MSD = $4D_e\Delta t$. As depicted in Figure 3(c), with the increase of the concentration of the urea solution, the diffusion coefficient showed an increasing trend, from 0.29 ± 0.01 $\mu m^2/s$ in the absence of urea to a maximum of 1.06 ± 0.05 $\mu m^2/s$ at a urea concentration of 300 mM (see Video S1 in the SI). This trend agrees with the fuel-dependent change of the average diffusion coefficient by the DLS measurement based on the Stokes−Einstein equation (see Figure S11(a) in the SI). The diffusion coefficient distribution also shows a continuous shift to the right with an increase of urea concentration (see Figure S11(b) in the SI). With a similar method, we characterized the motion behavior of Pt motors whose tracking trajectories without and with H_2O_2 fuel of varied concentrations are presented in Figure 3(d). The corresponding MSD plots certify that the movement of Pt motors is enhanced an increase in the H_2O_2 fuel concentration (Figure 3(e)). The D_e value was found to be 0.44 ± 0.02 $\mu m^2/s$ without fuel and then gradually increased to 1.59 ± 0.1 $\mu m^2/s$ at 5 wt % H_2O_2 (see Video S2 in the SI). From the DLS measurements, the average diffusion coefficient of the Pt motors shifts to the right continuously to higher values (see Figure S11(c, d) in the SI). The results of DLS and MSD analysis are consistent. Both methods indicate the effective self-propulsion of the two motors in corresponding fuels.

The active propulsion of the magnetic motors was achieved by utilizing a self-built magnetic field generating device based on electromagnetic coils. By applying an external gradient magnetic field, the magnetic MNMs can be remotely driven by a magnetic attracting force and move toward the direction of the magnetic field gradient.[47] Motion trajectories of the magnetic motors under different magnetic field intensities are shown in Figure 3(g). When the initial magnetic field intensity is 10.2 mT, the magnetic motors moved slowly and traveled a short distance in the same time interval due to the small attraction force. However, even though the speed of the magnetic motors is very small, the movement behavior has been changed from random Brownian motion to directional motion. With the strength of the magnetic field increasing, the speed of the nanomotor continues to increase and the trajectory becomes longer with the same time interval. As presented in Figure 3(h), the MSD plots of the magnetic motors show a parabolic shape, indicating that the nanomotors moved in a preferred direction under the action of a magnetic field force (see Video S3 in the SI). Moreover, the average speed of the magnetic motors demonstrates a linear relationship, with the magnetic field intensity increasing from 10.2 mT up to 20 mT. We demonstrate that the magnetic motors can be effectively activated by an external magnetic field, which allows for future magnetic manipulation on the nanomotors for even formation of swarming and also collective behavior for targeted transportation.[48]

Engine Switching of Nanomotors by Supramolecular Host−Guest Assembly and Disassembly. Although micro/nanoarchitectures of various materials and shapes have been widely explored as a carrier platform for the preparation of numerous MNMs,[49] the propelling nanoengines (e.g., catalytic- or magnetic-responsive components or moieties) are usually permanently "fixed" onto the surface of these MNMs by either chemical bond linkage or physical deposition/adsorption. Therefore, the disassembly and replacement of these nanoengines could hardly be realized, which greatly limits the adaptability of these MNMs in practical use. Azobenzene molecules (guest) have the characteristic of light-responsive isomerization between *cis* and *trans* configurations. Four possible mechanisms have been proposed for the photoisomerization of azobenzene, including rotation, reversal, concerted inversion, and reversal-assisted rotation.[50] However, only *trans* isomers of azobenzene can assemble with β-cyclodextrins to form host−guest complexation, whereas *cis* isomers cannot because they are much more polar and sterically hindered from complexation.[51] Such a property sheds light on the possibility that the nanomotors can realize mechanical dismantling and replacement of the driving nanoengines at the molecular level, mimicking macroscopic machines. As shown in Figure 4(a), we conducted a complete switching cycle of the nanoengine from β-CD@Urease to β-CD@Pt and *vice versa*. The motion behavior of different motors during the whole switching process was first characterized by DLS and motion tracking experiments (Figure S12 in the SI). As depicted in Figure 4(b, c), the diffusion coefficient of the initial urease motors was 0.75 ± 0.02 $\mu m^2/s$ in the absence of urea and increased to 0.96 ± 0.05 $\mu m^2/s$ in a 300 mM urea solution. This result is also in agreement with that determined from the slope of the linear fitting curves of average MSD plots of the initial urease motors (Figure S12(a, d) in the SI), indicating active self-propulsion of the biocatalytically driven nanomotors. Then, we irradiated the urease motors with UV light to facilitate the conversion of azobenzene molecules from *trans* to *cis* isomers to achieve disassembly of the urease engine. In order to verify whether the urease engine was detached, we characterized the zeta potential of the urease motors before and after the disassembly of the engine, which changed from −11 mV of HMSNP-Urease to 0.3 mV of HMSNP-Azo (*cis* isomers) (Figure S13(a) in the SI). The significant change of the surface charge proves the urease engine was indeed dismounted from the surface of the HMSNPs.

Next, to test whether the nanoengines can be reassembled onto the carriers, we added a Pt engine into the obtained HMSNP-Azo (*cis* isomers) after removal of the urease engine in the previous step. Upon irradiation with visible light, the azobenzene molecules would switch from *cis* to *trans* isomers, to complex with β-CD on the Pt engine again to form Pt motors. Subsequently, we characterized the motion behavior of Pt motors after switching Pt engines within corresponding fuels to confirm the effectiveness of the nanoengine replacement. As presented in Figure 4(d, e), the diffusion coefficient of the reassembled Pt motors increased from 0.83 ± 0.04 $\mu m^2/s$ in the absence of H_2O_2 to 1.18 ± 0.02 $\mu m^2/s$ in 0.5 wt % H_2O_2 solution, and the diffusion coefficient distribution correspondingly shifts to the right of the higher value range. Meanwhile, the diffusion coefficient value is 0.63 ± 0.02 and 1.01 ± 0.03 $\mu m^2/s$ in the absence of fuel and with 0.5 wt % H_2O_2 solution, respectively (Figure S12(b, e) in the SI), which also shows a clear tendency of enhanced movement. Furthermore, the zeta potential changed from 0.3 mV of HMSNP-Azo to −28 mV of HMSNP-Pt again (Figure S13(a) in the SI), which proves that the Pt engine was successfully

https://doi.org/10.1021/jacs.1c04836
J. Am. Chem. Soc. 2021, 143, 15063−15072

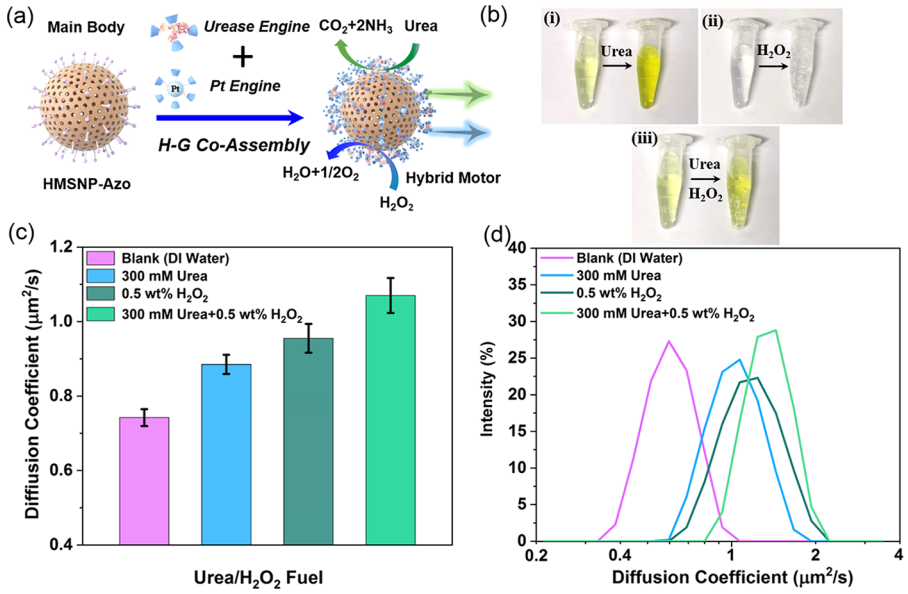

Figure 5. Construction and motion behavior characterization of a hybrid nanomotor of HMSNP-Pt&Urease by coassembly of dual nanoengines. (a) Schematic illustration of the fabrication and self-propelling of the hybrid nanomotor. (b) Biocatalytic/catalytic activity test of the hybrid nanomotor: (i) only urea fuel, (ii) only H_2O_2 fuel, and (iii) both urea and H_2O_2 fuels. Diffusion coefficient values (c) and distribution (d) of the hybrid nanomotor under different fuel conditions by DLS measurement. Error bars indicate standard deviation (N = 10).

assembled on the surface of HMSNPs through the host−guest interaction. The above results proved that we could achieve a nanoengine replacement to switch an enzymatic urease motor to a catalytic Pt motor with the aid of remote light control. Finally, to verify that the engine switching process can be reversed, we repeated the disassembly and reassembly process to replace the Pt engine with a urease engine again. Similarly, we characterized the motion behavior of urease motors after reassembling the urease engine again. Figure 4(f, g) and Figure S12(c, f) in the SI demonstrate that the recovered urease motors could achieve active propulsion in urea solution, which is consistent with the diffusion coefficient of the original urease motors too. In addition, zeta potential measurements traced the surface evolution of the functional moieties from −28 mV of the HMSNP-Pt to −18.5 mV of HMSNP-Azo to −9.7 mV of the recovered HMSNP-Urease nanomotors (Figure S13(b) in the SI), which agrees well with the zeta potential value of the initial urease motors and indicates successful switching of the nanoengines again. Here, the zeta potential of HMSNP-Azo was still negative, which may be because the β-CD@Pt nanoparticles were not completely detached or still partially entrapped in the mesoporous channels of the HMSNPs. In order to better understand the whole switching process, we summarize the molecular mechanism of the cyclic switching of the nanoengine. First, based on two molecular states of azobenzene, *trans* and *cis* isomers, the two states can be interconverted with the irradiation of different wavelengths of light. Second, upon UV light excitation, the azobenzene molecule on urease motors undergoes a $\pi-\pi^*$ transition and switches from the original *trans* state to the *cis* state, which induces the disassembly of inclusion complexes of β-CD and azobenzene molecules to detach and remove the initial loaded nanoengine of β-CD@Urease. Then, further treatment with visible light could reverse the *cis* isomer back to *trans* by an n−π^* transition, which allows for assembling the new β-CD@Pt nanoengines to obtain Pt motors. Third, the β-CD@Pt nanoengines can be disassembled and removed by converting azobenzene to *cis* isomers by UV light excitation again, and then the β-CD@Urease nanoengines can be assembled by restoring the *trans* isomers by visible light to complete the whole switching cycle of the nanoengine. The current findings presented here prove that by the means of host−guest supramolecular self-assembly, we can readily remove old nanoengines and install new ones, which enable great adaptability and universality for the construction of various MNMs on-demand.

Facile Construction of a Hybrid Nanomotor by Coassembly of Multiple Nanoengines. Hybrid MNMs with multiple propulsion modes can convert diverse forms of energies into kinetic force through different self-propelling mechanisms,[52,53] which is advantageous to overcome the shortcomings of short lifetime and low efficiency of a single propulsion mode. A number of hybrid MNMs of multiple propulsion functions, such as chemical-magnetic,[54] chemical-optical,[55] chemical-ultrasonic,[56] magneto-ultrasonic,[57] and electric-optical,[58] have been reported up to now. Inspired by these studies, we attempt to coassemble β-CD@Pt and β-CD@Urease nanoengines onto the main carrier (HMSNP-Azo) to prepare a dual-driven hybrid nanomotor (HMSNP-Pt&Urease), as shown in Figure 5(a). We anticipate that the hybrid nanomotor can be propelled either by H_2O_2 or by urea fuel individually or simultaneously fueled by both. First, three sets of qualitative tests of the biocatalytic/catalytic activities were conducted to verify the successful synthesis of the hybrid nanomotor. In Figure 5(b), in the former two tests, with only adding urea or H_2O_2 fuel, the light yellow color of the solution turned bright yellow due to the formation of NH_4^+ (Figure 5(b, i)) or generated vast bubbles (Figure 5(b, ii)) compared with the control group, indicating that the urease and Pt engines were successfully assembled on the surface of the HMSNP. In the third test, both urea and H_2O_2 fuel were added, the color change and bubble formation were both identified in the solution (Figure 5(b, iii)), indicating that hybrid nanomotors with dual engines can achieve both

https://doi.org/10.1021/jacs.1c04836
J. Am. Chem. Soc. 2021, 143, 15063−15072

biocatalytic and catalytic activities simultaneously. Here, the lighter color of the solution was caused by the bleaching effect of hydrogen peroxide added to the solution. Afterward, we characterized the motion behavior of the hybrid nanomotor. As shown in Figure 5(c), the diffusion coefficient of the hybrid nanomotor is only 0.74 ± 0.02 $\mu m^2/s$ without the addition of fuel. When 300 mM urea or a 0.5 wt % H_2O_2 solution was added individually, the corresponding diffusion coefficient increased to 0.89 ± 0.03 and 0.95 ± 0.05 $\mu m^2/s$, respectively. When the two fuels were added at the same time, the diffusion coefficient of hybrid nanomotors increased to 1.07 ± 0.04 $\mu m^2/s$, reaching the maximum value as compared to using only a single engine of either a urease (0.89 $\mu m^2/s$) or Pt engine (0.95 $\mu m^2/s$), proving that the hybrid nanomotors can achieve enhanced motion with a dual propulsion mode driven by both Pt and urease engines (see Video S4 in the SI). Moreover, it can be seen from Figure 5(d) that the diffusion coefficient distribution of the hybrid nanomotors also presents an apparent right-shift under each fuel condition. These results are generally consistent with the trend of average MSD plots of the hybrid nanomotor of HMSNP-Pt&Urease under different fuel conditions (Figure S13 in the SI). The current strategy based on supramolecular machine-based self-assembly provides a facile method for the construction of multi-engine-driven hybrid MNMs.

CONCLUSIONS

In conclusion, we develop a supramolecular machine-based strategy to construct nanomotors with detachable and replaceable engines, resembling assembling and dismounting of components/parts for macroscopic machines. We first synthesized the HMSNPs modified with photoresponsive azobenzene molecules (HMSNP-Azo) as the main carrier of the nanomotors. Nanomotors with different driving mechanisms were constructed separately via the formation of inclusion complexes between β-CD-modified engines (urease, Pt, or Fe_3O_4) and azobenzene on the carriers. The urease and Pt motors can achieve self-propulsion under the corresponding chemical fuels of urea and H_2O_2. Meanwhile, magnetic motors can be activated for directional propulsion by a gradient magnetic field. Taking advantage of light-responsive *cis*/*trans* isomerization of azobenzene molecules, the propelling engines preassembled on the carriers can be dismounted and exchanged with new ones to realize the engine switching of the nanomotors, which can hardly be achieved for traditional fabrication methods of MNMs such as chemical bonding or physical sputtering of catalytic components. Furthermore, multiple engines can be easily coassembled to form a hybrid nanomotor that can surmount individual propulsion regarding their propulsion capability. In addition, HMSNPs used here have a large specific surface, hollow structure, and good biocompatibility,[59] which bring merits for further development of nanomotor-based active and intelligent drug delivery systems, e.g., by combining molecular-based nanovalves or gatekeepers to realize stimuli-responsive drug release after reaching target sites in a biological environment.[60]

The concept of using supramolecular machine-enabled host−guest assembly of driving engines to build nanomotors provides a facile route to future multiple functionalizations of MNMs for on-demand task assignment, e.g., by assembling β-CD-modified functional moieties of biochemical sensing or drug delivery functions. Taking account of many other molecular machine-based molecular assembly structures such as using calixarene (CA) and cucurbituride (CB), as well as corresponding chemical or physical stimulus responsiveness to control their inclusion and disassociation, the current work opens a wide possibility of new designs of MNMs featuring much more complex functionalities that can be programmable at the molecular level.

ASSOCIATED CONTENT

Supporting Information

The Supporting Information is available free of charge at https://pubs.acs.org/doi/10.1021/jacs.1c04836.

Experimental details, SEM characterization of HMSNPs, FTIR and NMR spectra of carboxylated azobenzene, DLS data, FTIR spectra and zeta potential of β-CD@Urease, β-CD@Pt, and β-CD@Fe_3O_4, SEM-EDX mapping, diffusion coefficient and distribution, average MSD of the hybrid motor (PDF)

Video S1: Representative self-propulsion of an HMSNP-Urease nanomotor in different urea concentrations (AVI)

Video S2: Representative self-propulsion of an HMSNP-Pt nanomotor in different H_2O_2 concentrations (AVI)

Video S3: Representative self-propulsion of an HMSNP-Fe_3O_4 nanomotor under different magnetic field intensities (AVI)

Video S4: Representative self-propulsion of a hybrid nanomotor in different fuel concentrations (AVI)

AUTHOR INFORMATION

Corresponding Author

Xing Ma − *Sauvage Laboratory for Smart Materials, School of Materials Science and Engineering, Harbin Institute of Technology (Shenzhen), Guangdong, Shenzhen 518055, China; Shenzhen Bay Laboratory, Shenzhen 518055, China;* orcid.org/0000-0002-2248-4806; Email: maxing@hit.edu.cn

Authors

Zihan Ye − *Sauvage Laboratory for Smart Materials, School of Materials Science and Engineering, Harbin Institute of Technology (Shenzhen), Guangdong, Shenzhen 518055, China; Shenzhen Bay Laboratory, Shenzhen 518055, China*

Yong Wang − *Sauvage Laboratory for Smart Materials, School of Materials Science and Engineering, Harbin Institute of Technology (Shenzhen), Guangdong, Shenzhen 518055, China*

Sanhu Liu − *Sauvage Laboratory for Smart Materials, School of Materials Science and Engineering, Harbin Institute of Technology (Shenzhen), Guangdong, Shenzhen 518055, China*

Dandan Xu − *Sauvage Laboratory for Smart Materials, School of Materials Science and Engineering, Harbin Institute of Technology (Shenzhen), Guangdong, Shenzhen 518055, China*

Wei Wang − *Sauvage Laboratory for Smart Materials, School of Materials Science and Engineering, Harbin Institute of Technology (Shenzhen), Guangdong, Shenzhen 518055, China;* orcid.org/0000-0003-4163-3173

Complete contact information is available at: https://pubs.acs.org/10.1021/jacs.1c04836

Notes

The authors declare no competing financial interest.

■ ACKNOWLEDGMENTS

The authors thank the financial support from National Natural Science Foundation of China (52072095, 51802060), Shenzhen Science and Technology Program (JCYJ20020010-9113408066, KQTD20170809110344233), and Shenzhen Bay Laboratory (SZBL201906281005).

■ REFERENCES

(1) Ma, K. Y.; Chirarattananon, P.; Fuller, S. B.; Wood, R. J. Controlled Flight of a Biologically Inspired, Insect-Scale Robot. *Science* **2013**, *340* (6132), 603−607.
(2) Tu, Y.; Peng, F.; Adawy, A.; Men, Y.; Abdelmohsen, L. K. E. A.; Wilson, D. A. Mimicking the Cell: Bio-Inspired Functions of Supramolecular Assemblies. *Chem. Rev.* **2016**, *116* (4), 2023−2078.
(3) Solovev, A. A.; Xi, W.; Gracias, D. H.; Harazim, S. M.; Deneke, C.; Sanchez, S.; Schmidt, O. G. Self-Propelled Nanotools. *ACS Nano* **2012**, *6* (2), 1751−1756.
(4) Wang, Y.; Tu, Y.; Peng, F. The Energy Conversion behind Micro-and Nanomotors. *Micromachines* **2021**, *12* (2), 222.
(5) Xu, T.; Gao, W.; Xu, L.-P.; Zhang, X.; Wang, S. Fuel-Free Synthetic Micro-/Nanomachines. *Adv. Mater.* **2017**, *29* (9), 1603250.
(6) Gao, W.; Wang, J. Synthetic micro/nanomotors in drug delivery. *Nanoscale* **2014**, *6* (18), 10486−10494.
(7) Hu, M.; Ge, X.; Chen, X.; Mao, W.; Qian, X.; Yuan, W.-E. Micro/Nanorobot: A Promising Targeted Drug Delivery System. *Pharmaceutics* **2020**, *12* (7), 665.
(8) Luo, M.; Feng, Y.; Wang, T.; Guan, J. Micro-/Nanorobots at Work in Active Drug Delivery. *Adv. Funct. Mater.* **2018**, *28* (25), 1706100.
(9) Medina-Sánchez, M.; Xu, H.; Schmidt, O. G. Micro- and nano-motors: the new generation of drug carriers. *Ther. Delivery* **2018**, *9* (4), 303−316.
(10) Xu, D.; Wang, Y.; Liang, C.; You, Y.; Sanchez, S.; Ma, X. Self-Propelled Micro/Nanomotors for On-Demand Biomedical Cargo Transportation. *Small* **2020**, *16* (27), 1902464.
(11) Kong, L.; Guan, J.; Pumera, M. Micro- and nanorobots based sensing and biosensing. *Curr. Opin. Electrochem.* **2018**, *10*, 174−182.
(12) Yuan, K.; Bujalance-Fernández, J.; Jurado-Sánchez, B.; Escarpa, A. Light-driven nanomotors and micromotors: envisioning new analytical possibilities for bio-sensing. *Microchim. Acta* **2020**, *187* (10), 581.
(13) Srivastava, S. K.; Medina-Sánchez, M.; Koch, B.; Schmidt, O. G. Medibots: Dual-Action Biogenic Microdaggers for Single-Cell Surgery and Drug Release. *Adv. Mater.* **2016**, *28* (5), 832−837.
(14) Xi, W.; Solovev, A. A.; Ananth, A. N.; Gracias, D. H.; Sanchez, S.; Schmidt, O. G. Rolled-up magnetic microdrillers: towards remotely controlled minimally invasive surgery. *Nanoscale* **2013**, *5* (4), 1294−1297.
(15) Parmar, J.; Vilela, D.; Villa, K.; Wang, J.; Sánchez, S. Micro- and Nanomotors as Active Environmental Microcleaners and Sensors. *J. Am. Chem. Soc.* **2018**, *140* (30), 9317−9331.
(16) Ye, H.; Wang, Y.; Xu, D.; Liu, X.; Liu, S.; Ma, X. Design and fabrication of micro/nano-motors for environmental and sensing applications. *Appl. Mater. Today* **2021**, *23*, 101007.
(17) Wang, H.; Pumera, M. Fabrication of Micro/Nanoscale Motors. *Chem. Rev.* **2015**, *115* (16), 8704−8735.
(18) Wong, F.; Dey, K. K.; Sen, A. Synthetic Micro/Nanomotors and Pumps: Fabrication and Applications. *Annu. Rev. Mater. Res.* **2016**, *46* (1), 407−432.
(19) Ma, X.; Jannasch, A.; Albrecht, U.-R.; Hahn, K.; Miguel-Lopez, A.; Schaffer, E.; Sanchez, S. Enzyme-powered hollow mesoporous Janus nanomotors. *Nano Lett.* **2015**, *15* (10), 7043−7050.
(20) Tang, S.; Zhang, F.; Gong, H.; Wei, F.; Zhuang, J.; Karshalev, E.; Esteban-Fernández de Ávila, B.; Huang, C.; Zhou, Z.; Li, Z.; Yin, L.; Dong, H.; Fang, R. H.; Zhang, X.; Zhang, L.; Wang, J. Enzyme-powered Janus platelet cell robots for active and targeted drug delivery. *Sci. Robot.* **2020**, *5* (43), No. eaba6137.
(21) Shah, Z. H.; Wang, S.; Xian, L.; Zhou, X.; Chen, Y.; Lin, G.; Gao, Y. Highly efficient chemically-driven micromotors with controlled snowman-like morphology. *Chem. Commun.* **2020**, *56* (97), 15301−15304.
(22) Liu, W.; Ge, H.; Gu, Z.; Lu, X.; Li, J.; Wang, J. Electrochemical Deposition Tailors the Catalytic Performance of MnO_2-Based Micromotors. *Small* **2018**, *14* (45), 1802771.
(23) Zeeshan, M. A.; Grisch, R.; Pellicer, E.; Sivaraman, K. M.; Peyer, K. E.; Sort, J.; Özkale, B.; Sakar, M. S.; Nelson, B. J.; Pané, S. Hybrid Helical Magnetic Microrobots Obtained by 3D Template-Assisted Electrodeposition. *Small* **2014**, *10* (7), 1284−1288.
(24) Baraban, L.; Streubel, R.; Makarov, D.; Han, L.; Karnaushenko, D.; Schmidt, O. G.; Cuniberti, G. Fuel-Free Locomotion of Janus Motors: Magnetically Induced Thermophoresis. *ACS Nano* **2013**, *7* (2), 1360−1367.
(25) Gao, W.; Feng, X.; Pei, A.; Kane, C. R.; Tam, R.; Hennessy, C.; Wang, J. Bioinspired helical microswimmers based on vascular plants. *Nano Lett.* **2014**, *14* (1), 305−310.
(26) Chen, Y.; Xu, B.; Mei, Y. Design and Fabrication of Tubular Micro/Nanomotors via 3D Laser Lithography. *Chem. - Asian J.* **2019**, *14* (14), 2472−2478.
(27) Zhou, C.; Zhu, P.; Tian, Y.; Xu, M.; Wang, L. Engineering Micromotors with Droplet Microfluidics. *ACS Nano* **2019**, *13* (6), 6319−6329.
(28) Wu, Y.; Wu, Z.; Lin, X.; He, Q.; Li, J. Autonomous Movement of Controllable Assembled Janus Capsule Motors. *ACS Nano* **2012**, *6* (12), 10910−10916.
(29) Wu, Z.; Wu, Y.; He, W.; Lin, X.; Sun, J.; He, Q. Self-Propelled Polymer-Based Multilayer Nanorockets for Transportation and Drug Release. *Angew. Chem., Int. Ed.* **2013**, *52* (27), 7000−7003.
(30) Li, J.; Pumera, M. 3D printing of functional microrobots. *Chem. Soc. Rev.* **2021**, *50* (4), 2794−2838.
(31) Ma, X.; Hahn, K.; Sanchez, S. Catalytic Mesoporous Janus Nanomotors for Active Cargo Delivery. *J. Am. Chem. Soc.* **2015**, *137* (15), 4976−4979.
(32) Yu, J.; Wang, B.; Du, X.; Wang, Q.; Zhang, L. Ultra-extensible ribbon-like magnetic microswarm. *Nat. Commun.* **2018**, *9* (1), 3260.
(33) Leigh, D. A. Genesis of the Nanomachines: The 2016 Nobel Prize in Chemistry. *Angew. Chem., Int. Ed.* **2016**, *55* (47), 14506−14508.
(34) De Bo, G.; Gall, M. A. Y.; Kitching, M. O.; Kuschel, S.; Leigh, D. A.; Tetlow, D. J.; Ward, J. W. Sequence-Specific β-Peptide Synthesis by a Rotaxane-Based Molecular Machine. *J. Am. Chem. Soc.* **2017**, *139* (31), 10875−10879.
(35) Meng, Z.; Han, Y.; Wang, L.-N.; Xiang, J.-F.; He, S.-G.; Chen, C.-F. Stepwise Motion in a Multivalent [2](3)Catenane. *J. Am. Chem. Soc.* **2015**, *137* (30), 9739−9745.
(36) Zheng, Y. B.; Kiraly, B.; Huang, T. J. Molecular machines drive smart drug delivery. *Nanomedicine* **2010**, *5* (9), 1309−1312.
(37) Kim, J.; Piao, Y.; Hyeon, T. Multifunctional nanostructured materials for multimodal imaging, and simultaneous imaging and therapy. *Chem. Soc. Rev.* **2009**, *38* (2), 372−390.
(38) van Dijk, L.; Tilby, M. J.; Szpera, R.; Smith, O. A.; Bunce, H. A.; Fletcher, S. P. Molecular machines for catalysis. *Nat. Rev. Chem.* **2018**, *2* (3), 1−18.
(39) Ma, X.; Zhao, Y. Biomedical Applications of Supramolecular Systems Based on Host-Guest Interactions. *Chem. Rev.* **2015**, *115* (15), 7794−7839.
(40) Abendroth, J. M.; Bushuyev, O. S.; Weiss, P. S.; Barrett, C. J. Controlling Motion at the Nanoscale: Rise of the Molecular Machines. *ACS Nano* **2015**, *9* (8), 7746−7768.
(41) Feringa, B. L. In Control of Motion: From Molecular Switches to Molecular Motors. *Acc. Chem. Res.* **2001**, *34* (6), 504−513.
(42) Qi, G.; Wang, Y.; Estevez, L.; Switzer, A. K.; Duan, X.; Yang, X.; Giannelis, E. P. Facile and Scalable Synthesis of Monodispersed Spherical Capsules with a Mesoporous Shell. *Chem. Mater.* **2010**, *22* (9), 2693−2695.

https://doi.org/10.1021/jacs.1c04836
J. Am. Chem. Soc. 2021, 143, 15063−15072

(43) Vivero-Escoto, J. L.; Slowing, I. I.; Wu, C.-W.; Lin, V. S.-Y. Photoinduced intracellular controlled release drug delivery in human cells by gold-capped mesoporous silica nanosphere. *J. Am. Chem. Soc.* **2009**, *131* (10), 3462−3463.
(44) Yu, J.; Qu, H.; Dong, T.; Rong, M.; Yang, L.; Liu, H. A reversible light-responsive assembly system based on host-guest interaction for controlled release. *New J. Chem.* **2018**, *42* (8), 6532−6537.
(45) Llopis-Lorente, A.; Garcia-Fernandez, A.; Murillo-Cremaes, N.; Hortelão, A. C.; Patino, T.; Villalonga, R.; Sancenon, F.; Martinez-Manez, R.; Sanchez, S. J. A. n. Enzyme-powered gated mesoporous silica nanomotors for on-command intracellular payload delivery. *ACS Nano* **2019**, *13* (10), 12171−12183.
(46) Ma, X.; Wang, X.; Hahn, K.; Sánchez, S. Motion control of urea-powered biocompatible hollow microcapsules. *ACS Nano* **2016**, *10* (3), 3597−3605.
(47) Wang, Y.; Liu, Y.; Li, Y.; Xu, D.; Pan, X.; Chen, Y.; Zhou, D.; Wang, B.; Feng, H.; Ma, X. Magnetic Nanomotor-Based Maneuverable SERS Probe. *Research* **2020**, *2020*, 7962024.
(48) You, M.; Chen, C.; Xu, L.; Mou, F.; Guan, J. Intelligent micro/nanomotors with taxis. *Acc. Chem. Res.* **2018**, *51* (12), 3006−3014.
(49) Wang, C.; Wang, Q.; Dong, R.-F.; Cai, Y.-P. Dynamic self-assembly of micro-nanomotor. *Inorg. Chem. Commun.* **2018**, *91*, 8−15.
(50) Bandara, H. M. D.; Burdette, S. C. Photoisomerization in different classes of azobenzene. *Chem. Soc. Rev.* **2012**, *41* (5), 1809−1825.
(51) Lau, Y.; Ferris, D.; Zink, J., Photo-driven nano-impellers and nanovalves for on-command drug release. *SPIE*: **2010**; Vol. *7574*.
(52) Xiong, K.; Xu, L.; Lin, J.; Mou, F.; Guan, J. Mg-Based Micromotors with Motion Responsive to Dual Stimuli. *Research* **2020**, *2020*, 6213981.
(53) Feng, Y.; Yuan, Y.; Wan, J.; Yang, C.; Hao, X.; Gao, Z.; Luo, M.; Guan, J. Self-adaptive enzyme-powered micromotors with switchable propulsion mechanism and motion directionality. *Appl. Phys. Rev.* **2021**, *8* (1), 011406.
(54) Gao, W.; Manesh, K. M.; Hua, J.; Sattayasamitsathit, S.; Wang, J. Hybrid nanomotor: A catalytically/magnetically powered adaptive nanowire swimmer. *Small* **2011**, *7* (14), 2047−2051.
(55) Xing, Y.; Zhou, M.; Xu, T.; Tang, S.; Fu, Y.; Du, X.; Su, L.; Wen, Y.; Zhang, X.; Ma, T. Core@ Satellite Janus Nanomotors with pH-Responsive Multi-phoretic Propulsion. *Angew. Chem.* **2020**, *132* (34), 14474−14478.
(56) Ren, L.; Zhou, D.; Mao, Z.; Xu, P.; Huang, T. J.; Mallouk, T. E. Rheotaxis of Bimetallic Micromotors Driven by Chemical-Acoustic Hybrid Power. *ACS Nano* **2017**, *11* (10), 10591−10598.
(57) Li, J.; Li, T.; Xu, T.; Kiristi, M.; Liu, W.; Wu, Z.; Wang, J. Magneto-acoustic hybrid nanomotor. *Nano Lett.* **2015**, *15* (7), 4814−4821.
(58) Liang, X.; Mou, F.; Huang, Z.; Zhang, J.; You, M.; Xu, L.; Luo, M.; Guan, J. Hierarchical Microswarms with Leader-Follower-Like Structures: Electrohydrodynamic Self-Organization and Multimode Collective Photoresponses. *Adv. Funct. Mater.* **2020**, *30* (16), 1908602.
(59) Kankala, R. K.; Han, Y.-H.; Na, J.; Lee, C.-H.; Sun, Z.; Wang, S.-B.; Kimura, T.; Ok, Y. S.; Yamauchi, Y.; Chen, A.-Z.; Wu, K. C.-W. Nanoarchitectured Structure and Surface Biofunctionality of Mesoporous Silica Nanoparticles. *Adv. Mater.* **2020**, *32* (23), 1907035.
(60) Isa, E.; Ahmad, H.; Rahman, M.; Gill, M. R. Progress in Mesoporous Silica Nanoparticles as Drug Delivery Agents for Cancer Treatment. *Pharmaceutics* **2021**, *13* (2), 152.

https://doi.org/10.1021/jacs.1c04836
J. Am. Chem. Soc. 2021, 143, 15063−15072